Tunneling Modulation of Transistor Lasers: Theory and Experiment

Milton Feng, *Life Fellow, IEEE*, Junyi Qiu, *Senior Member, IEEE*, and Nick Holonyak, Jr., *Life Fellow, IEEE*

(*Invited Paper*)

***Abstract*— The coherent photons generated at the base quantum wells in the transistor laser (TL) interact with the collector field and "assist" electron tunneling from the valence band of the base to the conduction band states of the collector. The cavity coherent photon intensity effect on photon-assisted tunneling in the TL has resulted in the realization of a novel photon-field enhanced optical absorption. This intra-cavity photon-assisted tunneling (ICPAT) in the TL or the light-emitting transistor is the unique property of voltage (field) modulation and the basis for ultrahigh speed direct tunneling photon modulation and switching. In addition, a new tunneling current modulation gain in a "new form" of transistor is discovered based on the collector tunneling holes feedback to the base and dielectric relaxation base transport. The TL, owing to its unique three-terminal configuration and the complementary nature of its optical and electrical collector output signals, enables fast base recombination, collector tunneling, and OEO feedback, which has resulted in the realization of compact electro-optical applications, such as non-linear signal-mixing, frequency multiplication, OE tunneling transistor, and electrical and optical bistability.**

***Index Terms*— Transistor, diode laser, transistor laser, tunnel junction, carrier-photon dynamics, heterojunction bipolar transistor, stimulated and spontaneous recombination, microwave equivalent circuit model, analog and logic optoelectronic circuits, optical switch, resonance-free response, current and voltage modulation, feedback linearization, frequency multiplication, electrical and optical bistability.**

I. Introduction

TRANSISTOR was first invented by Bardeen and Brattain [1] in 1947 and revealed its fundamental operating principles: the emitter current injection, the base electron-hole recombination, and the collector current output due to base transport. Since then the three-terminal transistor has replaced the fragile vacuum tube for reliable and fast electrical signal switching and amplification, and enabled the integration of three-terminal transistors into microchips by Kilby [2], [4] and Noyce [3] and later of low power CMOS circuits into VLSI, which revolutionized the modern electronics and communication systems, creating the digital world we live in today. Subsequently, a wide bandgap emitter transistor was proposed by Shockley [5] and Kroemer [6] to improve the transistor's emitter injection efficiency, which created a heterojunction bipolar transistor (HBT) and marked the beginning of engineering semiconductor material structures to alter the device performance. The SiGe, GaAs, and InP heterostructure transistors have been widely deployed today in microwave and millimeter-wave power amplifiers for wireless communication and mixed signal ICs for high-speed ADC and testing instruments, with the cutoff frequency approaching terahertz regime [7].

Besides being fundamental to transistor operation, the electron-hole recombination process in alloy semiconductors has become a powerful light source as LEDs and semiconductor diode lasers. In a transistor's electrical operation, the base recombination serves primarily as a way to promote carrier transport and establish power amplification (gain); however, by enhancing recombination in a direct-bandgap alloy III-V compound semiconductor, efficient electron-photon conversion will happen, leading to the discovery of light-emitting diodes (LEDs) and diode lasers (1962) [8], [9], To further improve the radiative recombination efficiency, quantum wells (QWs) have been inserted into the recombination region (1977) [10], [11]. Today LEDs are the mainstream lighting source with low power consumption, low heating, and low cost.

The quantum-well diode laser, due to its miniature size compared with gas lasers, has opened many possibilities from cheap laser pointers to light detection and ranging (LiDAR) and 3D imaging. It has also become the critical part in high-speed optical communication systems commonly found in today's large-scale data centers: the exponential increasing volume of data motivates an increase in the system data rate, which causes electrical interconnects to incur increasing losses. At high data rates, it becomes more energy-efficient to convert electrical signals to optical signals using

Manuscript received December 31, 2017; accepted February 6, 2018. Date of publication February 27, 2018; date of current version March 13, 2018. This work was supported in part by Dr. Kenneth C. Goretta, Air Force of Scientific Research under Grant FA9550-15-1-0122, in part by Dr. Michael Gerhold of the Army Research Office under Grant W911NF-17-1-0112,in part by the Pao Family Fellowship, in part by the National Science Foundation under Grant 1640196, and in part by the Nanoelectronics Research Corporation, a wholly-owned subsidiary of the Semiconductor Research Corporation (SRC), through Electronic-Photonic Integration Using the Transistor Laser for Energy-Efficient Computing, an SRC-NRI Nanoelectronics Research Initiative through Research Task under Grant 2697.001.The work of M. Feng was supported by the N. Holonyak, Jr., Emeritus Chair of Electrical and Computer Engineering. The work of N. Holonyak, Jr., was supported by the John Bardeen Emeritus Chair (Sony) of Electrical and Computer Engineering and Physics. *(Corresponding author: Junyi Qiu.)*

The authors are with the Department of Electrical and Computer Engineering, Microelectronics and Nanotechnology Laboratory, University of Illinois at Urbana–Champaign, Champaign, IL 61801 USA (e-mail: mfeng@illinois.edu).

Color versions of one or more of the figures in this paper are available online at http://ieeexplore.ieee.org.

Digital Object Identifier 10.1109/JQE.2018.2809471

semiconductor lasers. Today's commercial high-speed optical transceivers running at 25 Gb/s per channel have become the backbone of global communication, and the demand will be even higher with the anticipation of the new 5G standard, the associated computation-intensive applications, and more recently the 3D sensors for face recognition.

In 2016, an uncooled oxide-VCSEL (vertical-cavity surface-emitting laser) demonstrated the record modulation bandwidth of 29 GHz and error-free data transmission at 57 Gb/s [12], [13]. Fundamentally, the modulation bandwidth of a diode laser is limited by the carrier recombination lifetime and the photon lifetime. Specifically, for the diode laser p-i-n junction structure, a low recombination lifetime can only be achieved by injecting a large number of carriers from the p and n side into the neutral junction region to reach lasing threshold, which in return will heat up the junction and slow down the carrier recombination; thus, the modulation bandwidth is thermally limited to < 35 GHz.

In 2004, Feng and Holonyak realized the radiative recombination at the base of a III-V semiconductor HBT can be modulated and the light output can be established as the new transistor optical output signal, and the light-emitting transistor (LET) was invented [14]. Soon the laser operation was also demonstrated by inserting QWs in the base [15] and providing an optical cavity to the LET; the transistor laser (TL) is realized [16], [17]. Different from diode lasers, in LET and TL the recombination center is in the HBT base region, which is heavily doped, carrier injection follows HBT operation principles: (1) carriers are injected from the emitter side, and the emitter-base heterojunction prevents hole leakage and improves the emitter injection efficiency; (2) the injected minority carriers diffuse across the heavily doped base; a portion recombine in the base (primarily in the undoped QWs) and converted into photons, and the remaining carriers reach the collector; the heavily doped base and QWs reduce the overall base recombination lifetime and therefore increase the base recombination current at the cost of lower transistor current gain; (3) the collector collects all the carriers that do not recombine and sweep them to the terminal. Thus, the LET and TL shift the focus of transistor operation from electrical (collector output) to optical (base recombination), and the base QWs can be treated as the optical equivalent of "collector", establishing the duo output (both electrical and optical) of the LET and TL.

As a result, the base carrier recombination lifetime can be reduced by manipulating the base doping, QWs, and the tilted charge distribution profile in the base region. The benefit of a tilted charge distribution can be shown in Fig. 1 where the TL base carrier profile is drawn schematically: electrons are injected and diffuse across the base active region, which has a thickness of around 100 nm and corresponds to a base transit time of ~ 2 ps given by the relation $\tau_t = W_B^2/2D$ with $D \approx 26$ cm^2/s.

Because the base transport process always competes with the base recombination process, a carrier that fails to recombine within picoseconds will inevitably diffuse to the collector. Thus, the transistor base region can filter all the slow-recombining carriers and effectively reduce the overall recombination lifetime. The result has been verified experimentally: (a) the LET has demonstrated a modulation bandwidth of 7 GHz which corresponds to a recombination lifetime of 23 ps [18] and far exceeds LED's record bandwidth at around 1 GHz; (b) the TL has demonstrated a nearly "resonance-free" frequency response over bias current range of I/I_{th} with a modulation bandwidth of 20 GHz [19] corresponding to a recombination lifetime of 29 ps, while the 57 Gb/s VCSELs are in the range of ~160 picoseconds [20]. The physics of the base carrier charge dynamics of the three-port transistor laser was also established [21], [22], and the microwave equivalent-circuit model is shown in Fig. 2.

Unlike in a diode laser where the population inversion is pinned at the lasing threshold and hence its lasing state fixed, the population inversion in a TL is governed by the base and the collector charging, hence it is able to shift its operation in preference of a particular mode with a higher differential gain [23]. This behavior can be utilized to extract the differential optical gain from the collector I-V characteristics, a key parameter to the high-speed performance of a laser, which for a single-QW TL is found to be 100 times larger than in a diode laser [24].

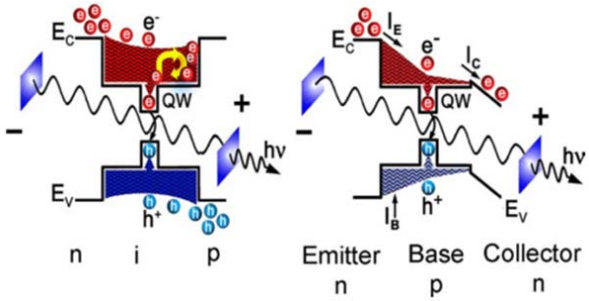

Fig. 1. Pictures show schematically the active region e-h carrier distribution profile in (a) a diode laser and (b) a transistor laser; in transistor laser the carrier distribution is "tilted" due to the base diffusion carrier transport.

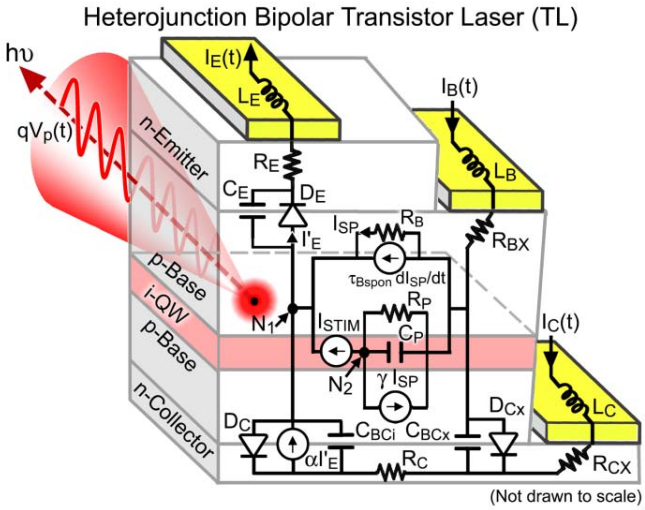

Fig. 2. Physics-based model of a three-port heterojunction bipolar transistor laser (TL) formulated in equivalent-circuit electrical and optical elements to simulate the base current modulation.

The advantage of the TL's three-terminal structure is also demonstrated in the use of the collector current as a negative feedback signal for linearization of both the optical and electrical output signals [25]. The three-terminal advantage is further revealed by the TL's ability to introduce structural enhancements, e.g. a tunnel junction at the collector to improve voltage-controlled signal modulation via photon-assisted tunneling [26]. The simultaneous base current and collector voltage modulation of a tunnel-junction TL enables non-linear signal mixing and frequency multiplication up to the 11^{th} order above lasing threshold [27]. Two detailed review papers of three-port transistor laser have been reported [28], [29].

II. Tunneling in Transistor Laser

A. Photon-Assisted Tunneling (PAT)

The electric field-dependence of the fundamental absorption edge of a semiconductor is ordinarily referred to as the Franz-Keldysh effect [30]–[32]. For a direct-gap semiconductor, photon absorption in a *p-n* junction can often be thought of simply as photon-assisted tunneling over the energy gap. That is, the electron wavefunctions in the valence and the conduction bands have exponentially decaying tails in the energy gap. In the presence of an electrical field, a valence band electron may tunnel through a triangular barrier to reach the conduction band. When photons are present, the electron can absorb the energy of a photon, effectively reducing the tunneling barrier height by the photon energy, thus the tunneling probability is significantly enhanced and the probability depends on the electric field as well as the photon energy. Such photon absorption process due to photon-assisted tunneling (PAT) has been studied within *p-n* junction diodes [33], [34] and is well-known as an electro-absorption phenomenon for the photodiodes.

B. Intra-Cavity Photon-Assisted Tunneling (ICPAT)

It has been discovered that a similar PAT process can also happen inside the cavity of LETs and TLs: photons generated from the base QWs will experience the electric field in the collector junction controlled by the junction reverse bias and thus promote the base valence band electrons to tunnel to the collector conduction band. This observation suggests the cavity tunneling modulating the LET and TL optical output directly by collector voltage. In 2007, the TL employing intra-cavity PAT (ICPAT) was demonstrated and achieved the tunneling modulation and switching operation from stimulated (under high coherent field) to spontaneous (incoherent field) [35]. Later in 2009, a tunnel-junction TL demonstrated direct voltage-controlled modulation using collector ICPAT [36], and the absorption coefficient incorporated into the laser coupled rate equations [37]. In 2016, the internal loss resulting from bias-dependent PAT in a TL of low and high cavity Q was reported [38]. Later, the difference between ICPAT and PAT was clarified, and the field-dependence of the tunneling absorption rate was quantified. Previous studies of PAT have been limited to *p-n* junctions with external illumination, i.e., the case of a photodetector [31], [32]. When PAT happens in the TL collector junction, the coherent photon absorption is enhanced inside the cavity, and the laser output modulation is much faster due to the presence of cavity reflection [37]. Finally the rebalance of carriers by base dielectric relaxation in response to tunneling was discovered and studied [39], [40], leading to the formulation of the TL tunneling operations and formally establishing LETs and TLs as four-port devices with both electrical (*I-V*) and optical (*L-V*) outputs as functions of the base current and the collector voltage.

Thus, the collector plays an integral role in the operation of the TL. Its close proximity to the base active region allows it to be used as a direct readout of the transport and recombination dynamics in the base and QWs. High $p+$ and $n+$ doping can be employed at the collector to form a tunnel junction and control the laser operation more effectively by changes in the junction bias (voltage), which makes possible a direct (circuit) scheme of voltage modulation in addition to the usual one of current modulation. Moreover, the recombination optical signal, via internal ICPAT optical absorption, causes voltage-dependent breakdown and negative resistance in the TL collector characteristics, which are particularly advantageous for signal processing. The collector tunnel junction is an additional source of hole re-supply to the base and to the base recombination, complementing and competing with the usual base current supply I_B. Now the LETs and TLs can be viewed as a device-level integration of two photonics functions: photon generation (with base QWs) and photon absorption (with collector junction tunneling via PAT or ICPAT), and they have the potential to achieve more complex functions involving both the electrical and the optical signal simultaneously and can potentially find applications in photonic integrated circuits.

III. Tunneling Modulation of Optical Output in Transistor Laser

A. Energy Band Diagram of a Transistor Laser

The schematic energy band diagram of a heterojunction TL (*n-p-n*) with quantum wells (QWs) in the base, ICPAT at the collector junction, and a reflecting optical cavity is shown in Fig. 3. The device operates with emitter current injection, base recombination and transport, and tunneling collector current output. The base recombination hole current (I_{Br}) is supplied by the external base current (I_B), the ICPAT hole current ($I_{ICPAT,h}$), and the band-to-band direct tunneling hole current (I_{rT}). The collector electron current (I_C) comprises the base electron current reaching the collector junction (I_t), the ICPAT electron current ($I_{ICPAT,e}$), and the band-to-band direct tunneling electron current (I_{rT}). The photon generation is due to *e-h* recombination at the base QWs, and the photon absorption is due to ICPAT tunneling at the collector junction. The corresponding hole current contributes to the base for electron relaxation transport and excess (injected) carrier spontaneous and stimulated recombination, thus providing at the collector the tunneling-modulation of the laser and tunneling-amplification of the transistor [39], [40]. The cleaved mirrors provide the optical cavity and assist to build up coherent laser output when the cavity photon density is above the coherent threshold. Figure 4 shows a fabricated quantum-well TL.

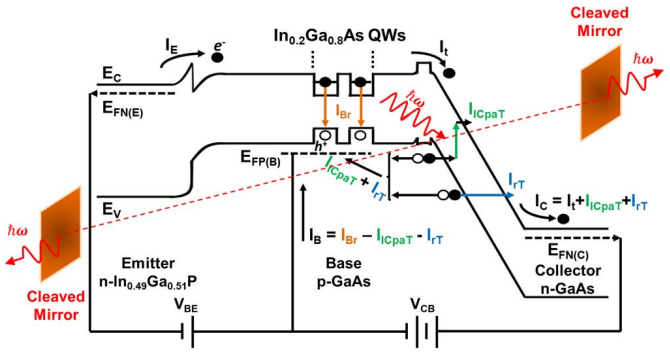

Fig. 3. Schematic diagram of a quantum-well (QW) transistor laser operating by e-h recombination in the base QWs and photon absorption by intra-cavity photon-assisted tunneling (ICPAT) at the collector junction. The collector current $I_C = I_t + I_{ICPAT} + I_{rT}$ where $I_t = \beta_1 \times I_B + \beta_2 \times (I_{ICPAT} + I_{rT})$. The current gains are defined in Section IV (B).

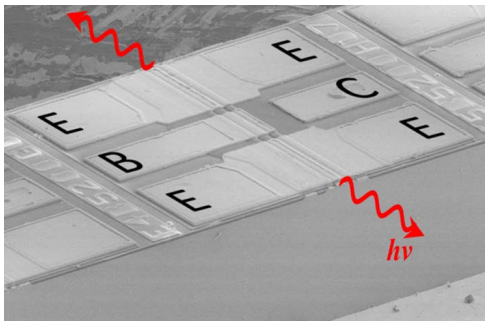

Fig. 4. Scanning electron microscopy of the top view of a fabricated QW edge-emitting transistor laser with cavity length L = 200 μm.

Different from the transistor invented by Bardeen and Brattain (1947) with the base operating only in *e-h* spontaneous recombination, the transistor laser of Feng and Holonyak (2004) possesses both *e-h* spontaneous and stimulated recombination in the base QWs, both incoherent and coherent photon generations in base QWs, and photon absorptions in the collector via ICPAT. The collector tunneling modulation of the photon density inside the TL optical cavity also provides a hole current to the total base recombination (Optical-Electrical (OE) feedback modulation control) and results in the lowering of the emitter junction barrier. Thus, an induced minority electron current, injected from the emitter to the base near the collector junction via dielectric relaxation transport in femtoseconds, provides tunneling current gain for the transistor [39], [40].

B. Coupled Carrier-Photon Rate Equations in Transistor Laser

The coupled carrier-photon dynamics of the TL are obtained by integrating the continuity equations of the minority carriers (Eqn. (1) and (2)) over the entire base region and by further relating the spontaneous and stimulated optical outputs to the respective components of the total base recombination current. This results in the coupled carrier-photon rate equations:

$$\frac{dP}{dt} = v\Gamma g P - \frac{P}{\tau_p} \tag{1}$$

and

$$\frac{dN}{dt} = \frac{I_E}{q} - \left(\frac{I_C}{q} + \frac{N}{\tau_{B,spon}} + vg\Gamma P\right) \tag{2}$$

Here P is the total photon population, v is the photon group velocity in the optical cavity, Γ is the confinement factor to normalize the active medium (QW) over the entire cavity, τ_p is the photon lifetime, g is the gain of the active medium, and $N \approx (Q_1 + Q_2)/q$ is the total minority carrier population in the base. The formula has the same structure as the one first formulated by Statz and deMars (1960) [37]. These equations for the TL show that the photon generation is governed by the rate of the transport of minority carriers (electrons) in the base, because the hole density does not change appreciably in the heavily p-doped base of an *n-p-n* heterojunction transistor. In contrast, both electrons and holes are minority carriers in the undoped active region of a *p-i-n* diode laser, the rate of *e-h* recombination is governed by the rate of transport of both electrons and holes.

The optical output frequency response of the TL is obtained from the coupled rate equations by expressing N as $N = N_o + \delta N(\omega)$, $P = P_o + \delta P(\omega)$, and $I_B = I_{B,o} + \delta I_B(\omega)$. The first order small-signal solution of the coupled carrier-photon rate equations is given in Eqn. (3),

$$\frac{\Delta P_m}{\Delta I_B} = \frac{\frac{v_g \Gamma P_0}{qAW_B}\frac{\partial g}{\partial N}}{\left[\frac{1}{\tau_p}\left(v_g\Gamma\frac{\partial g}{\partial N}P_0\right) - \omega^2\right] + j\omega\left(\frac{1}{\tau_b} + v_g\Gamma\frac{\partial g}{\partial N}P_0\right)} \tag{3}$$

where ΔI_B is the small signal base current, ΔP_m is the small signal photon density, P_o is the steady-state photon density, A is the device area, Γ is the optical confinement factor, v_g is the photon group velocity, q is the electron charge, W_B is the transistor laser base width, $\partial g/\partial N$ is the differential optical gain, τ_p is the photon lifetime, and τ_b is the spontaneous carrier lifetime.

C. Coupled Carrier-Photon Rate Equations in Transistor Laser With Intra-Cavity Photon Assisted Tunneling

For simplicity, we may assume ICPAT shares the same closed-form solution as PAT $\sim F^{1/3}\int_{C/F^{2/3}}^{\infty}|Ai(z)|^2 dz$, where F is collector junction electrical field, and C is a constant determined by the QW and collector junction.

The coupled rate equations are then modified to include ICPAT photon absorption, α_{ICPAT}. Further note that as drawn in Fig. 3, $I_C = I_t + I_{rT} + I_{ICPAT} \sim I_C(\alpha_{ICPAT}, P)$ because $I_{ICPAT}/q = v\alpha_{ICPAT}P$ where P is the cavity photon population and v is the cavity photon group velocity, and the minority carrier injection, $I_E = I_E(I_C)$, is coupled to the collector current, I_C, as a result of the tunneling re-supply of holes to the base. The coupled rate equations can then be expressed as:

$$\frac{dP}{dt} = v\left(\Gamma g - \alpha_i - \alpha_m - \alpha_{ICPAT}\right)P \tag{4}$$

and

$$\frac{dN}{dt} = \frac{I_E(I_C)}{q} - \frac{I_C(\alpha_{ICPAT}, P)}{q} - \frac{N}{\tau_{B,spon}} - v\Gamma g P \tag{5}$$

By considering small-signals, the minority carrier population, $N = N_o + \delta N(\omega)$; for the optical gain, $g = g_o + (\partial g/\partial N) \cdot \delta N(\omega)$; the photon population, $P = P_o + \delta P(\omega)$; the expressions $I_E = I_{E,o} + \delta I_E(\omega)$; $I_C = I_{C,o} + \delta I_C(\omega)$; $\alpha_{ICPAT} = \alpha_{ICPAT,o} + \delta\alpha_{ICPAT}(\omega)$; and the triode current constraint, $\delta I_E(\omega) = \delta I_C(\omega) + \delta I_B(\omega)$. Equations (4) and (5) may be written in small-signal nonlinear form as

$$j\omega\delta P = \Gamma v P_o \frac{\partial g}{\partial N}\delta N - v P_o \delta\alpha_{ICPAT} + \Gamma v \delta P \delta N - v\delta\alpha_{ICPAT}\delta P \quad (6)$$

and

$$j\omega\delta N = \frac{\delta I_B}{q} - \frac{\delta N}{\tau_{B,spon}} - \Gamma v g_o \delta P - \Gamma v P_o \frac{\partial g}{\partial N}\delta N - \Gamma v \delta P \delta N \quad (7)$$

with $\delta\alpha_{ICPAT}$ expanded in Taylor series below as shown in Eqn. (8):

$$\delta\alpha_{ICPAT} = \left.\frac{\partial\alpha_{ICPAT}}{\partial V_{CB}}\right|_{V_{CB,O}} \delta V_{CB} + \left.\frac{\partial^2\alpha_{ICPAT}}{\partial V_{CB}^2}\right|_{V_{CB,O}} \delta V_{CB}^2 + \ldots + \left.\frac{\partial^m\alpha_{ICPAT}}{\partial V_{CB}^m}\right|_{V_{CB,O}} \delta V_{CB}^m + \ldots \quad (8)$$

The mixing terms $[\delta I_B(f_1)]^m \cdot [\delta V_{CB}(f_2)]^n$ generate the output mixing frequencies $mf_1 \pm nf_2$, and can be derived recursively. First, the linear solution is obtained from Eqn. (6) and (7) by neglecting the nonlinear terms involving $\delta\alpha_{ICPAT} \cdot \delta P$ and $\delta N \cdot \delta P$, which gives $\delta P = R_{PI}(\omega)\delta I_B + R_{PV}(\omega)\delta V_{CB}$, where $R_{PI}(\omega)$ and $R_{PV}(\omega)$ are the current and voltage modulation coefficients respectively. Higher order mixing terms such as $\delta I_B \cdot \delta V_{CB}$, $(\delta I_B)^2 \cdot \delta V_{CB}$, $\delta I_B \cdot \delta V_{CB})^2$, etc., are obtained by retaining all the mixing terms and substituting the expression for δP into in Eqn. 6 and 7 at each recursive step. The tunnel junction produces the nonlinear (coupling) term, $\delta P \cdot \delta\alpha_{ICPAT}$, without which the nonlinearity can only come from current modulation, i.e., only $\delta P \cdot \delta N$.

D. Tunneling Modulation of Light in a Transistor Laser

In a two-terminal semiconductor light-emitting device such as LED, diode laser, or VCSEL, the light output depends solely on the injected current. However, a three-terminal light-emitting device such as LET or TL, the light output is a function of both the injected base current (I_B) and the collector junction bias (V_{CB} or V_{CE}). The TL with stimulated recombination in the base and ICPAT in the collector junction thus has a special set of light output (L-I_B-V_{CE}, L = light output power; $V_{CE} = V_{CB} + V_{BE}$, V_{BE} is constant at given I_B) family of curves as shown in Fig. 5.

In the regime where V_{CB} is small and the collector junction has not reached strong reverse bias, the laser output (proportional to the cavity photon density) increases with emitter electron injection into the base. The stimulated recombination then saturates limited by the hole supply by base current I_B. Once the collector junction reaches sufficient reverse bias, ICPAT occurs, and the laser output is reduced as shown in Fig. 5. Further increasing V_{CB} and reducing the photon density inside the cavity will break the lasing threshold condition, causing coherent breakdown with the coherent light output dropping to zero.

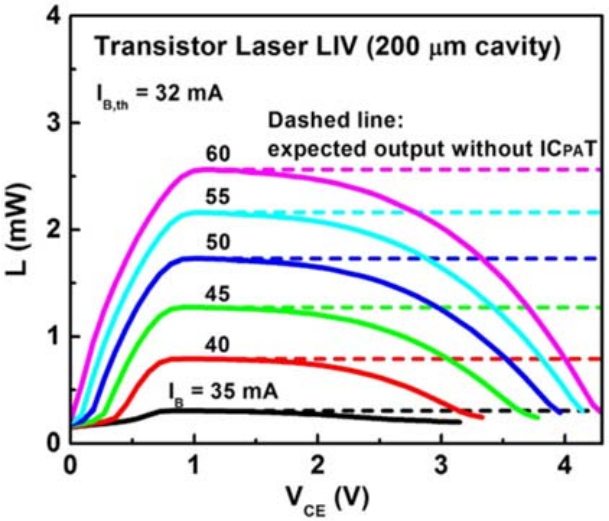

Fig. 5. TL optical output (coherent) as a function of both the base current and the collector bias. The optical output drops at high bias due to ICPAT. Without ICPAT, the optical output is expected to be proportional to the base current and saturate at high collector voltage.

The current-driven diode laser optical output characteristic equation is:

$$L_{DL} = \frac{\hbar\omega}{q}\eta_i \frac{\alpha_m}{\alpha_i + \alpha_m}(I - I_{th}) \quad (9)$$

Following the same format, we recognize the collector ICPAT as an additional cavity loss term and incorporate it in the above equation to formulate the TL output equation:

$$L_{TL} = \frac{\hbar\omega}{q}\eta_i \frac{\alpha_m}{\alpha_i + \alpha_m + \Gamma\alpha_{ICPAT}}(I - I_{th,ICPAT}) \quad (10)$$

where α_{ICPAT} accounts for the photon absorption through ICPAT, Γ is a confinement factor since ICPAT only happens at the collector junction, and $I_{th,ICPAT}$ incorporates the fact that the laser threshold is directly proportional to the total cavity loss (thus dependent on ICPAT). Note that as the collector junction bias V_{CB} changes, both α_{ICPAT} and $I_{th,ICPAT}$ will change, and we observe the unique ability to modulate the cavity loss in a TL through ICPAT. When ICPAT is negligible, $\alpha_{ICPAT} = 0$ and $I_{th,ICPAT} = I_{th}$, and the TL behaves like a diode laser.

Based on Eqn. (9) and (10), the amount of light output reduction (ΔL) can be obtained by subtracting the expected output without ICPAT (dashed lines) and the actual observed output (solid lines) as shown in Fig. 5. The light output without ICPAT is predicted to be constant and independent of V_{CB} in the reverse bias V_{CB} regime, where a saturated collector current persists with a constant base current supplying holes to the base. Thus we have:

$$\Delta L = L_{DL} - L_{TL} = L_{DL} - \frac{\hbar\omega}{q}\eta_i \frac{\alpha_m}{\alpha_i + \alpha_m + \Gamma\alpha_{ICPAT}}\left(I - I_{th,ICPAT}\right) \quad (11)$$

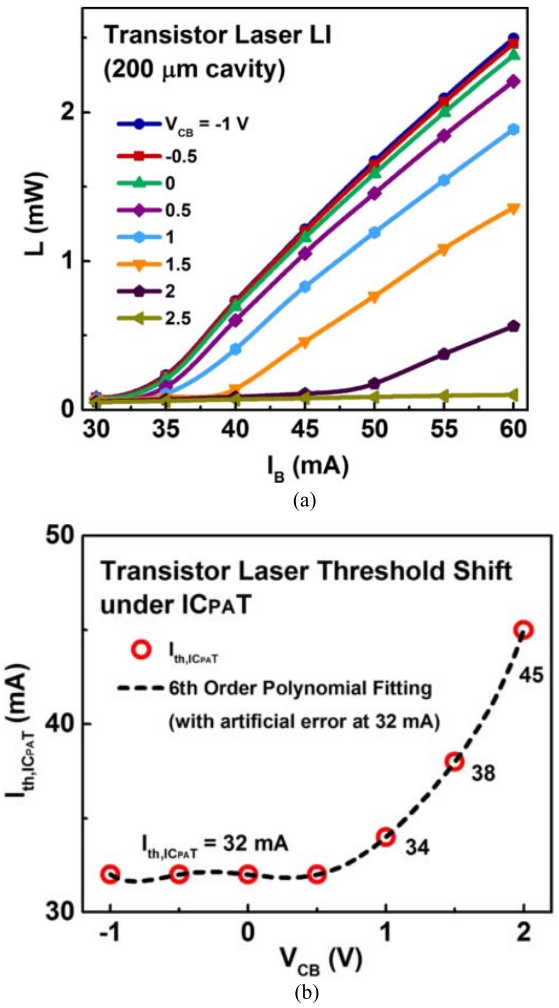

Fig. 6. (a) TL optical output plotted against the base current (L-I_B) to show the increase of lasing threshold with respect to the collector bias, and (b) the TL lasing threshold plotted against the collector junction bias. The lasing threshold shows a strong voltage dependence because the ICPAT process contributes to an additional cavity loss term as shown in Eqn. 10. Thus the TL demonstrates the unique ability to modulate the cavity photon loss with tunneling collector voltage.

With 980 nm emission wavelength from the InGaAs quantum wells in the base region, $hv = 1.265\ eV$, $\alpha_m \approx 59\ cm^{-1}$ (uncoated cleaved facet, 200 μm cavity), and $\alpha_i \approx 2\ cm^{-1}$ from results published at NTU [38]. A series of conversion efficiency η_i values can be obtained by examining the light output at $V_{CE} = 1\ V$ from the L-I_B-V_{CE} curves where the light output is at maximum. The TL threshold under ICPAT as a function of collector junction voltage V_{CB} can be found by plotting the light output versus the base current as shown in Fig. 6.

E. ICPAT Enhanced Optical Absorption

The product of the ICPAT optical absorption coefficient and the confinement factor, $\Gamma\alpha_{ICPAT}$, can be calculated based on the derivations in Section (D) and the result is plotted in Fig. 7. The optical absorption coefficient due purely to PAT (α_{PAT}) is also computed using established formulas [31], [32] and plotted for comparison.

The confinement factor Γ requires a more careful treatment. Different from the definition of confinement in

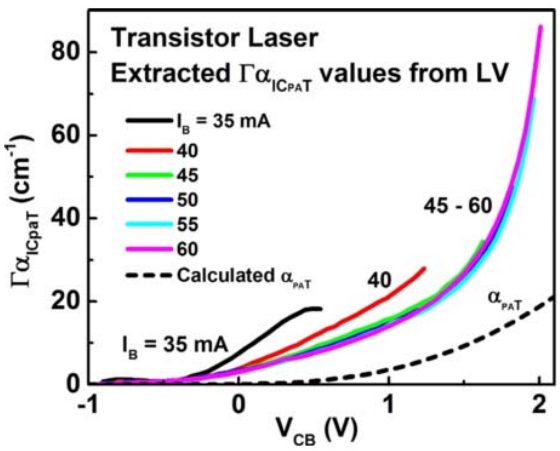

Fig. 7. TL ICPAT optical absorption coefficient normalized by the confinement factor as a function of the collector junction bias. The absorption coefficient of PAT is also plotted for reference. The absorption coefficient increases with voltage because the tunneling process is field-dependent; the absorption coefficient decreases with base current because of increased degree of coherence inside cavity.

the quantum-well gain medium, the Γ here represents the normalization of the ICPAT absorption region (collector junction) to the entire photon occupation region. The TL device has a 120 nm emitter, 100 nm base, and 100 nm collector confined by the optical waveguide; thus Γ is estimated to be at most 30%. We acknowledge it is $\Gamma\alpha_{ICPAT}$ that affects the photon absorption and do not separate the terms. The extracted $\Gamma\alpha_{ICPAT}$ values show a dependence on I_B above $I_{th} = 32\ mA$. The absorption coefficient decreases with increasing I_B up to 45 mA ($I/I_{th} = 1.4$) at a given V_{CB} and saturates when $I_B > 50\ mA$. This indicates the coherent photon density inside the cavity will disturb the cavity photon-electrodynamics and affect the particle tunneling process. Specifically, the result shows ICPAT absorption is more likely at low I_B levels (low photon density, $I/I_{th} < 1.5$). With low photon field near the lasing threshold, the cavity mode distribution is broader and less coherent, thus the absorption coefficient higher. As the photon field increases, the mode distribution is narrower and approaches coherent; thus, the absorption coefficient lower.

The higher-order modes generated by the QWs are at increasing polarizations with respect to the fundamental mode. The shift of the mode distribution has been reported for a 400 μm transistor laser [41]. The higher order modes are more pronounced at lower current injection levels, and the dominant mode rises quickly with increasing base current injection. The change of the injected base current I_B effectively shifts the photon mode distribution and the degree of coherence inside the cavity. The higher-order modes can pass through the absorption junction multiple times due to the misalignment of propagation direction along the transverse direction, which effectively increases the absorption coefficient. This also explains the low optical absorption under ICPAT for a high-Q cavities with a mirror coating [40]. Again, the dependence of the optical absorption coefficients on the photon field within the laser cavity is not accounted for by PAT as formulated by Franz-Keldysh, justifying the different treatment here of ICPAT.

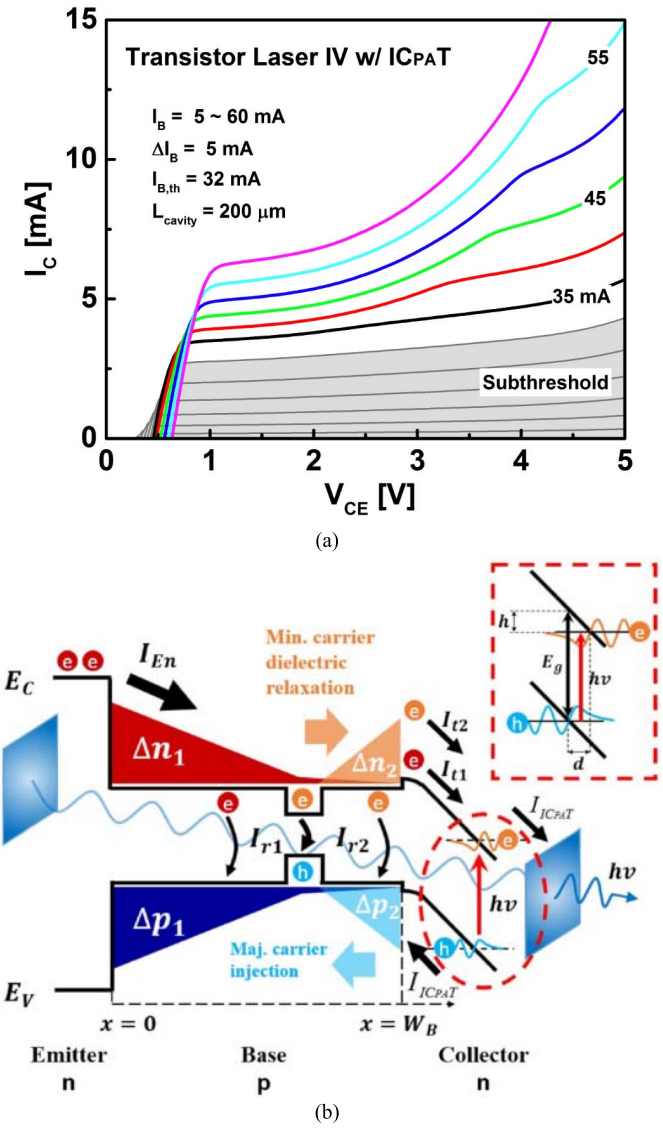

Fig. 8. (a) TL electrical output I_C-V_{CE} family curves showing the collector current increase due to ICPAT; (b) TL band diagram explaining the collector current increase when ICPAT happens: electrons tunnel from the base valence band to the collector conduction band and contribute to the total collector drift current (I_{ICPAT}). Additionally, the hole creation and accumulation in the base valence band (Δp_2) will draw more electrons from the emitter through dielectric relaxation and create an additional base transport current I_{t2}.

IV. Tunneling Modulation of Currents in Transistor Laser

A. Tunneling Modulation of Currents in Transistor Laser

A similar analysis was conducted on the TL electrical outputs [40]. Figure 8(a) shows the TL *I-V* characteristic with collector current I_C as the electrical output. Unlike the conventional transistor *I-V* behavior, the TL collector current will increase significantly with junction bias due to ICPAT and tunneling current gain, and the conventional transistor saturation region is almost absent as the TL is in the lasing state ($I > 32\ mA$).

B. Collector Tunneling, Base Dielectric Relaxation Transport and Tunneling Transistor Current Gain

This behavior can be explained by ICPAT: as the tunneling rate increases with the collector junction electric field, more electrons will tunnel from the base valence band to the collector conduction band and contribute to the total collector current. As shown in Fig. 8 (b), we denote the TL base recombination current as I_{r1}, the emitter-to-collector transport current I_{t1}, and the tunneling current as I_{ICPAT}. Holes created by tunneling will drift into the base as a base tunneling injection current I_{ICPAT} and contribute to the total base recombination as I_{r2}. Under steady-state operation, the base tunneling hole injection current I_{ICPAT} is equal to I_{r2} to maintain a constant hole accumulation density Δp_2 near the collector junction. The hole accumulation Δp_2 will break the charge balance in the base and consequently lower the emitter-base energy potential barrier to allow more emitter electrons to enter the base via dielectric relaxation transport, causing an electron accumulation Δn_2 to appear near the collector junction to balance Δp_2. The electron accumulation Δn_2 will inevitably drift to the collector and contribute to the 2nd base transport current I_{t2}.

Thus, we have:

$$I_C = I_{C0} + \Delta I_C = I_{t1} + I_{t2} + I_{ICPAT} \tag{12}$$

where I_{C0} is the collector current when ICPAT is negligible, ΔI_C is the increase of collector current under ICPAT, I_{t1} is the emitter-to-collector transport current under normal transistor operation, and I_{t2} is the emitter-to-collector dielectric relaxation transport current under ICPAT. Coupled with Eqn. (10), this set of equations describes the duo output (electrical and optical) characteristics of the TL tunneling operation.

To quantify the tunneling current, we denote the normal transistor current gain as:

$$\beta_1 = I_C / I_B \approx I_{t1} / I_{r1} \tag{13}$$

We further define a tunneling current gain β_2 to account for the tunneling-induced carrier transport associated with Δn_2 and Δp_2:

$$\beta_2 = I_{t2} / I_{r2} = I_{t2} / I_{ICPAT} \tag{14}$$

We may interpret β_2 in two ways: in the I_{t2}/I_{r2} form, it describes the base transport factor when the emitter electrons respond to the charge accumulation in the base; in the I_{t2}/I_{ICPAT} form, it describes how many more electrons are brought to the collector for every photon absorbed during ICPAT, i.e., the photon-electron conversion gain (a lower bound estimate since the quantum efficiency of ICPAT may not be one). Thus, the increase of the total collector current under ICPAT becomes:

$$\Delta I_C = I_{t2} + I_{ICPAT} = (\beta_2 + 1) \cdot I_{ICPAT} \tag{15}$$

The tunneling current I_{ICPAT} can be obtained by calculating the photon absorption rate while converting to the electron generation rate assuming a unity quantum efficiency. The tunneling gain β_2 can then be extracted and the result is shown in Fig. 9(a).

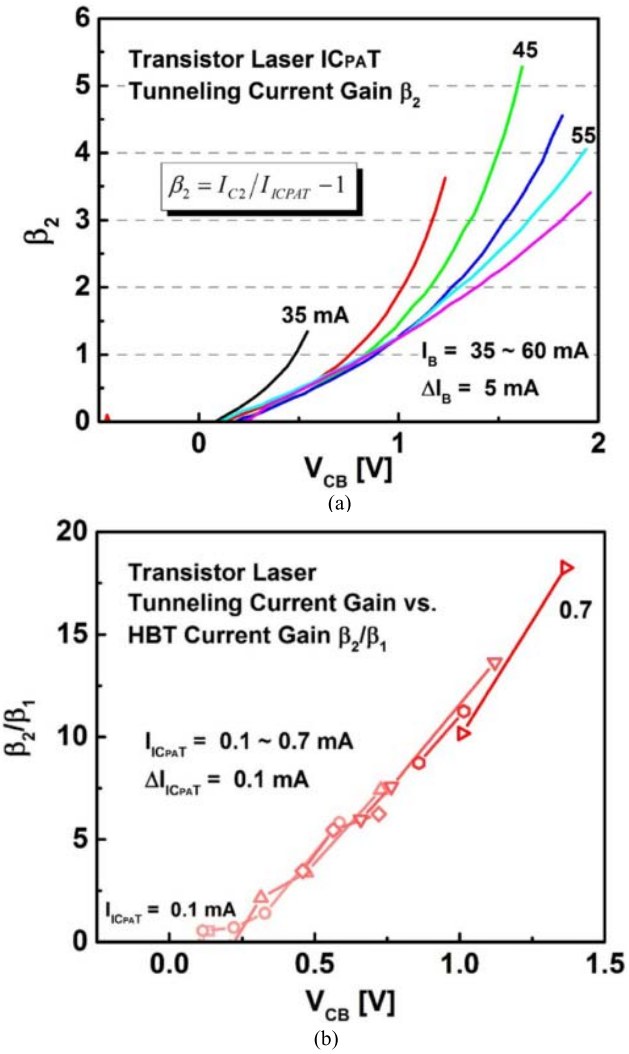

Fig. 9. (a) TL tunneling current gain β_2 as a function of the collector junction bias; the tunneling gain increases with junction bias because of increased ICPAT process with respect to the junction electric field; the tunneling gain decreases with base current because of reduced base recombination lifetime at higher base current level; (b) The ratio of the TL tunneling current gain β_2 to the normal transistor current gain β_1 as a function of the junction bias; at high bias, the tunneling amplification gain increase can be as high as 18 times.

Note that β_2 is always greater than zero as long as the collector junction is under reverse bias, indicating that each absorbed photon in the collector junction by ICPAT can produce more than one electron at the collector terminal, thus justifying the term "tunneling gain". Since $\beta_2 = I_{t2}/I_{r2}$ and I_{r2} is inversely proportional to the base recombination lifetime, β_2 will increase with V_{CB} for a given base current I_B because the base recombination lifetime will increase due to the loss of photons at higher V_{CB}. The tunneling gain will decrease with increasing base current at given V_{CB} because a higher base current will reduce the base recombination lifetime.

The ratio of the tunneling current gain β_2 to the normal transistor current gain β_1 is shown in Fig. 9(b). The 18x enhancement is due to the fast electron transport through the base region via dielectric relaxation. In a normal transistor, the injected minority electrons are delayed by the base transit time (τ_{tB}) to reach the collector. However, in the TL with ICPAT, the minority electrons respond to the injected majority holes and can reach the collector via dielectric relaxation. For typical TLs, the base is doped to $\sim 2\times10^{19}\ cm^{-3}$ and the resistivity is calculated to be $\sim 4.3\times10^{-3}\ \Omega\cdot cm$; thus, the dielectric relaxation time is estimated to be $\tau = \varepsilon_r\varepsilon_0\rho = 4.9\ fs$. Hence the electrical signal delay under tunneling operation is limited approximately by the carrier drifting time at the collector junction and the base recombination lifetime at the base, as both the ICPAT tunneling time ($\sim 20\ fs$) and the dielectric relaxation time ($\sim 5\ fs$) are negligible.

Concluding this section, we have identified and formulated the TL tunneling operation principles: ICPAT will prevail at high collector voltage bias, reducing the optical output while increasing the electrical output. The amount of optical output reduction is determined by the ICPAT absorption coefficient, which is affected by the junction electric field strength and the cavity photon coherency; for each photon absorbed, more than one electron is generated at the electrical output, the ratio of which is governed by the tunneling gain β_2. This is explained by the dielectric relaxation transport of carriers in response to the tunneling process disturbing the charge neutrality in the base region. We thus observe the tunneling process profoundly modifying the TL optical and electrical outputs, and we establish it as the basis for the ultrafast TL tunneling modulation.

Finally, we summarize the different derivations of the transistor current gain from Bardeen's transistor to the TL with and without tunneling operation. The Bardeen's transistor current gain β_1, defined by the ratio of the base current input modulation to the collector current output, and the use of the charge-control model in the base can be expressed as:

$$\beta_1 = \frac{I_C}{I_B} = \frac{Q/\tau_{EC}}{Q/\tau_B} = \frac{\tau_B}{\tau_{EC}} = \frac{\tau_{bulk}}{\tau_{tB}+\tau_{drift}} \tag{16}$$

In Eqn. (16), τ_{bulk} is the bulk base recombination lifetime which is inversely proportional to the base majority carrier concentration, τ_{EC} is the emitter-to-collector minority carrier transit time, which can be separated into τ_{tB} the base transit time, and τ_{drift} the carrier drift time at the collector junction. For a high-speed HBT structure with very thin base (small τ_{tB}), the collector junction drift time τ_{drift} needs to be accounted for.

When QWs are added to the transistor base, the total base carrier recombination lifetime τ_B can be further reduced [15]. Thus the QW transistor current gain $\beta_{1QW(spon)}$ is derived as:

$$\beta_{1\,QW(spon)} = \frac{\tau_B}{\tau_{tB}+\tau_{drift}} = \frac{\frac{1}{\frac{1}{\tau_{bulk}}+\frac{Q_1}{Q_2}\frac{1}{\tau_{t,EQW}}}}{\tau_{tB}+\tau_{drift}} \approx \frac{\frac{Q_2}{Q_1}\tau_{t,EQW}}{\tau_{tB}+\tau_{drift}} \tag{17}$$

In Eqn. (17), Q_1 is the base storage charge for QW recombination, Q_2 is the base stored charge for the collector transport, and $\tau_{t,EQW}$ is the base transit time from the emitter to the QW. The numerator in Eqn. (17) describes the reduction of the total base recombination lifetime τ_B due to the QW fast recombination lifetime of $(Q_2/Q_1)\tau_{t,EQW}$. Note that in this case the spontaneous recombination dominates.

In the TL operation, the base recombination lifetime τ_B is further reduced due to the QW shifting from spontaneous to stimulated recombination, which analytically takes the form of:

$$\beta_{1\,QW(stim)} = \frac{\tau_B}{\tau_{tB} + \tau_{drift}} = \frac{\frac{1}{\frac{1}{\tau_{bulk}} + \frac{Q_1}{Q_2}\frac{1}{\tau_{stim}} + \frac{Q_1}{Q_2}\frac{1}{\tau_{t,EQW}}}}{\tau_{tB} + \tau_{drift}} \approx \frac{\frac{Q_2}{Q_1}\tau_{stim}}{\tau_{tB} + \tau_{drift}} \tag{18}$$

In Eqn. (18), the stimulated recombination lifetime τ_{stim} is proportional to the cavity photon density.

For the TL under tunneling operation, the transistor current gain $\beta_{1QW(stim)}$ is the same as Eqn. (18); the tunneling current gain $\beta_{2(tunnel)}$ can be expressed as:

$$\beta_{2(tunnel)} = \frac{I_{t2}}{I_{r2}} = \frac{q\Delta n_2 v_{drift}}{\frac{1}{2}\frac{L_{QW} q \Delta p_2}{\tau_{stim}}} = \frac{v_{drift}}{\frac{1}{2}\frac{L_{QW}}{\tau_{stim}}} = \frac{\frac{L_C}{\tau_{drift}}}{\frac{1}{2}\frac{L_{QW}}{\tau_{stim}}} \approx \frac{\frac{L_{QW}}{L_C}\tau_{stim}}{\tau_{drift}} \tag{19}$$

In Eqn. (19), L_{QW} is the distance from the QW to the base-collector junction and L_C is the length of the collector junction. The tunneling current gain β_2 is approximately the ratio of the QW stimulated recombination lifetime to the carrier drift time at collector junction, which can explain the observation in Fig. 9(a).

V. Applications of Tunneling Modulation

A. Tunneling Modulation of Light Output in Edge Emitting Transistor Laser (EETL)

The previous sections have established the TL tunneling modulation on both the optical and electrical outputs: the optical output can be efficiently suppressed by ICPAT which is field-dependent and more pronounced than PAT, and the electrical output can be enhanced by ICPAT which brings more than one electron to the collector output for every tunneling electron. In both cases, the ultimate limit to the modulation speed is the tunneling time, indicating the TL under tunneling operation has an ultra-high inherent speed.

The first demonstration of the tunneling modulation on the TL optical output was in 2007 [34]. The TL is biased at a constant base current level (38 mA) and constant V_{CE} at 1.8, 2.2, and 2.6 V, respectively; V_{CE} is modulated with a 200 mV peak-to-peak square-wave at 1 GHz frequency. The optical output is shown in Fig. 10. Note at higher V_{CE} (or equivalently,V_{CB}) the TL optical output will drop significantly due to ICPAT, thus the optical output signal-to-noise ratio at $V_{CE} = 2.6\ V$ (Fig. 10(c)) is very low.

B. Tunneling Modulation of Light Output in Vertical Cavity Transistor Laser (VCTL)

Following the development of oxide-confined edge-emitting diode laser (EEDL) and VCSEL [17]–[21], the possibility of using a vertical structure for the transistor laser (VCTL) on oxide confined npn structure to improve efficiency was explored and demonstrated at 80°K [42]. Room temperature operation of pnp structure of VCTL was first demonstrated [43]. The schematic device diagram of an oxide-confined vertical cavity transistor laser (VCTL) is shown in Fig. 11 (a). The lateral oxidation layer underneath the emitter metal for current and optical confinement is achieved by trench opening and deep oxidation. The scanning electron microscopy image of a selectively oxidized VCTL with an active area of $7 \times 5\ \mu m^2$ is shown in Fig. 11 (b).

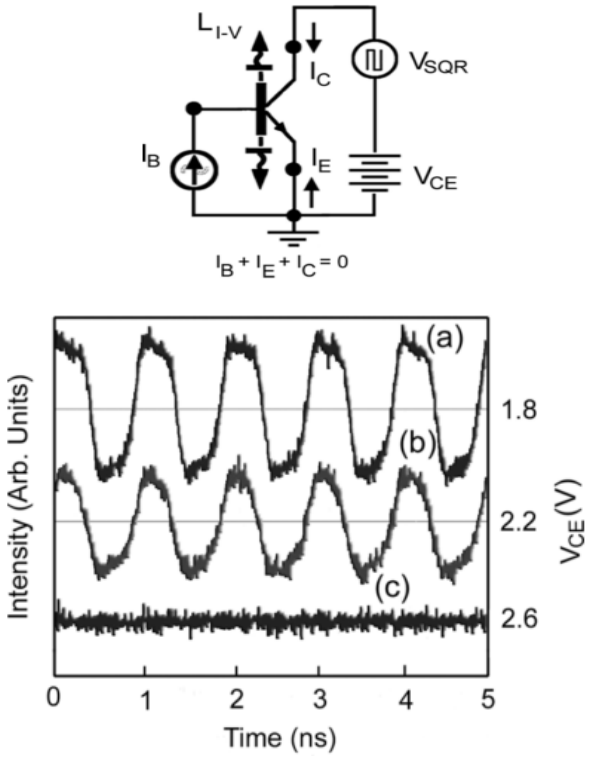

Fig. 10. Circuit schematic showing the TL tunneling modulation experiment setup, and the TL optical output under tunneling modulation at different V_{CE} biases: (a) 1.8, (b) 2.2, and (c) 2.6 V; the input is a 200 mV peak-to-peak square-wave at 1 GHz frequency. The optical output response decreases with increasing V_{CE} due to ICPAT reducing the cavity photon density.

The oxide-confined VCTL yields better electrical and optical confinement and leads to a higher cavity Q compared with the edge-emitting structure. The emission spectra of a $4.7 \times 5.4\ \mu m^2$ VCTL at $I_B = 2, 3$, and 4 mA are shown in Fig. 12. When $I_B = 2\ mA$, the magnified ($\times 100$) spontaneous spectrum shows three distinct peaks near 968 nm. When $I_B > I_{B,TH}$, the fundamental mode dominates. The inset shows in log scale the lasing peak at 970.96 nm with a side-mode suppression ratio (SMSR) of 31.76 dB and a full-wave half-maximum (FWHM) of 0.23 $\AA$ (corresponding to Q = 42,216) at $I_B = 4\ mA$ and $V_{CE} = 5\ V$.

We proceed to demonstrate the microwave bandwidth of a selective-oxide confined VCTL employing both current and voltage modulation. Figure 13 shows the measured modulation responses of a VCTL at three different biases at 80 K (common-emitter setup). In addition to the usual direct current modulation at the base-emitter (BE) port, the VCTL can also be directly voltage-modulated at the collector-emitter (CE) port. The light emission is collected by a fiber

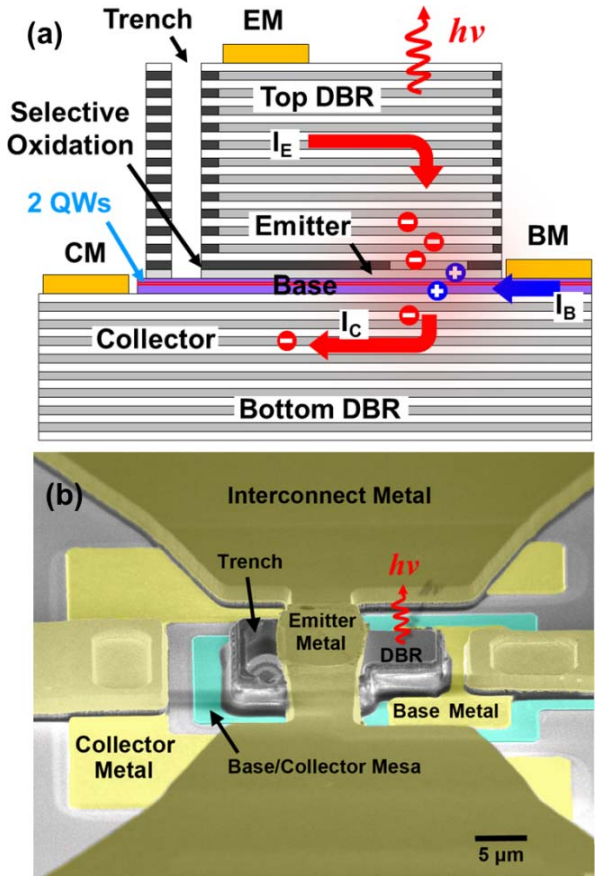

Fig. 11. (a) Schematic of an oxide-confined VCTL; (b) SEM top view of 7×5 um^2 VCTL showing the emission region and the trench opening region used for oxidation.

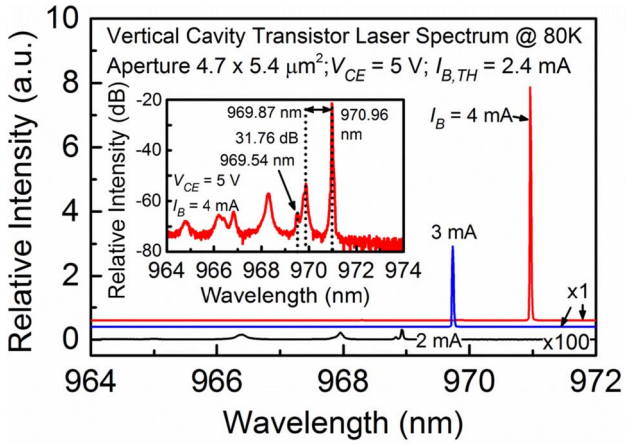

Fig. 12. The emission spectra of a 4.7×5.4 um^2 VCTL.

and coupled into a high-speed photodetector. At $V_{CE} = 3.5\ V$ and $I_B = 1.5 \times I_{B,TH} = 3.6\ mA$, the device operates in the saturation mode with both BE and BC junction in forward bias. Similar to diode laser, the carriers injected from the two junctions will pile up in the active region and the storage charge accumulated delays the QW recombination and consequently the signal switching, resulting in a lower bandwidth at $f_{-3dB} = 6\ GHz$. When the device is biased at $V_{CE} = 5\ V$ and$I_B = 3.6\ mA$, the BC junction becomes

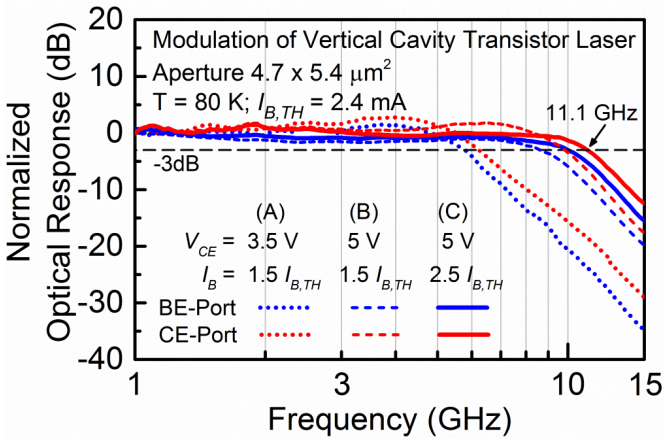

Fig. 13. Resonance-free optical responses of the microwave modulated common-emitter VCTL are measured with base-emitter (BE) current input (blue) or collector-emitter (CE) voltage input (red) at three different biases. A $f_{-3dB} = 11.1\ GHz$ resonance-free optical response is demonstrated.

reverse-biased and the device operates in the forward active mode. The tilted charge distribution in the base region (no carrier pile-up effect) reduces the storage charge, which is forced by the reverse-bias BC junction boundary condition and allows the transistor to have fast *e-h* recombination lifetime and operate at a higher speed with a nearly resonance-free frequency response curve. Thus, a higher bandwidth of $f_{-3dB} = 9\ GHz$ is obtained. Further increasing the cavity photon density by raising $I_B/I_{B,TH} = 2.5$ enhances the f_{-3dB} to 11.1 *GHz*, which is obtained at $V_{CE} = 5\ V$ and $I_B = 6\ mA$. Note that the typical diode laser's resonance peak (due to slow e-h recombination and charge pile up) is absent from the device's optical output frequency response under both base-current or collector-voltage modulation up to 11 *GHz*, despite the high emitter resistance of 603 Ω. In all cases, the VCTL under collector-voltage tunneling modulation has demonstrated higher bandwidth than under current modulation. With further reduction of parasitic and device scaling, the VCTL can become the ideal laser source for high-speed and high-signal integrity data communication.

C. Signal Mixing and Frequency Multiplication with a Tunneling Transistor Laser [37]

Above-threshold signal mixing is made possible by the nonlinear coupling of the high internal coherent optical field ($h\nu$) to the base electron-hole recombination (I_B), minority carrier (electron) emitter-to-collector transport (I_E), and the base-to-collector electron tunneling (I_{ICPAT}) at the collector junction. The coherent photons generated at the QW via electron-hole recombination interact with the collector junction field (V_{CB}) and assist electron tunneling from base to collector, resulting in a hole re-supply current (I_{ICPAT}) into the base region and a reduction in the coherent optical field (photon absorption). In addition, unique to the transistor, the positively charged holes re-supplied to the base will raise the electrical potential of the base and reduce the base-emitter potential difference (V_{BE}), causing minority electrons to be injected into the base from the emitter (I_E).

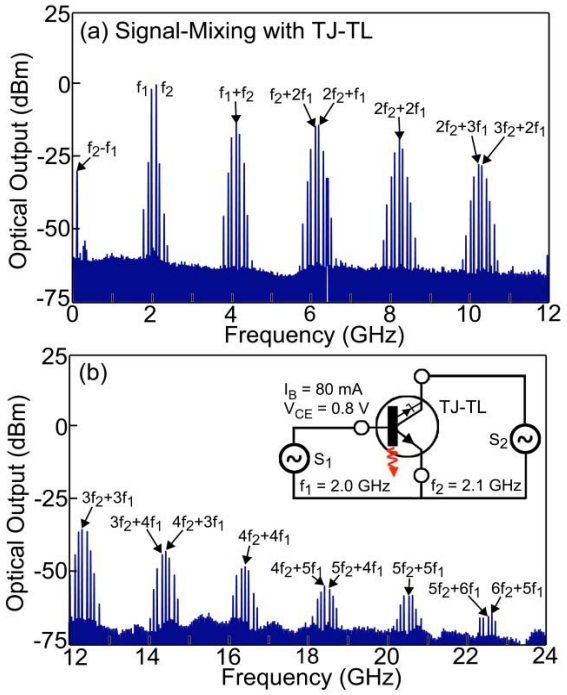

Fig. 14. Signal mixing experiment results with a tunnel junction TL in the common-emitter configuration, producing optical output with harmonics at $mf_1 \pm nf_2$. The input tones are of equal RF power (0 *dBm*) at 2 and 2.1 *GHz*.

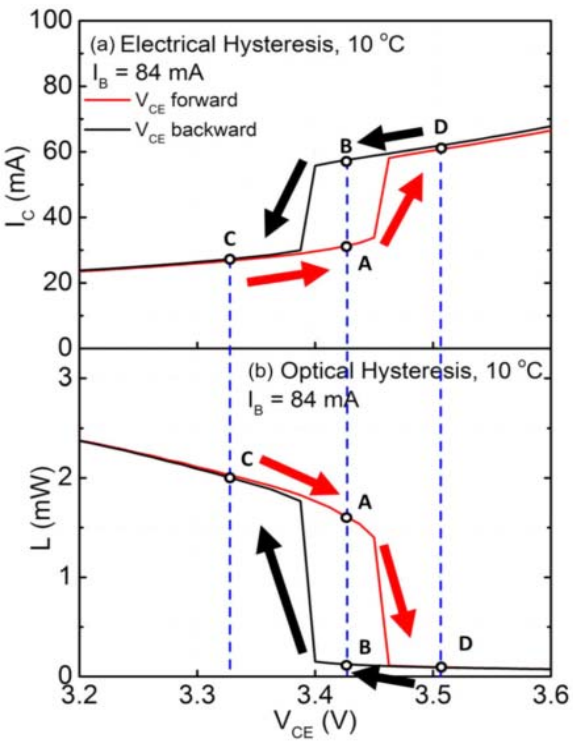

Fig. 15. The TL electrical I_C-V_{CE} and optical L-V_{CE} hysteresis at 10 °C. When V_{CE} increases from 3.33 to 3.43 V, the I_C and L (red) move forward from point (C) to (A); I_C increases, and L drops because of increased tunneling at higher collector junction bias, but the optical output is still in the coherent emission state with the TL base operates in stimulated recombination. When V_{CE} further increases from 3.43 to 3.51 V, the I_C and L (red) move forward from point (A) to (D); the optical output eventually shifts from coherent to incoherent state when the cavity photon density drops below the coherent threshold ($V_{TU} = 3.46$ V in this case) and the TL base operates in spontaneous recombination, thus the sudden decrease of L. The sudden increase of I_C is due to the higher transistor current gain when the base recombination rate is reduced.

The current amplification ($\delta I_E/\delta I_{ICPAT}$) is possible depending on the transistor structure. This, together with a change in the coherent optical field, results in a change in the minority carrier population in the base region (and QWs), and hence, in the stimulated and spontaneous electron-hole recombination rate (I_B). Furthermore, ICPAT is known to exhibit a highly nonlinear absorption behavior as a function of the collector junction bias V_{CB}, shown in Fig. 7.

A three-terminal tunnel-junction TL, when used as a nonlinear microwave device, is much more convenient for circuit matching. It utilizes the nonlinearity from the strong coupling between the minority carrier injection (I_E), the electron-hole recombination (I_B), and the collector junction field (V_{CB}), mediated by ICPAT (I_{ICPAT}) at the collector junction. Figure 14 shows the signal mixing outputs of a tunnel-junction TL with $f_1 = 2$ *GHz* applied to the BE port and $f_2 = 2.1$ *GHz* applied to the CE port (tunnel junction); harmonics up to 20 *GHz* are observed. The tunnel-junction TL therefore emerges as a new nonlinear signal processing (adding and mixing) device operating above laser threshold for improved optical output power. It can serve as a powerful nonlinear optoelectronic component for applications such as frequency multiplication, frequency synthesis, and signal processing.

D. Tunneling Modulation for Optical and Electrical Bistability in Transistor Laser [44]

The inherent electron-photon coupling mechanism in the TL implies the electrical and optical outputs are strongly coupled as well. Figure 15 shows the TL electrical I_C-V_{CE} and optical L-V_{CE} curves at 10 °C. When V_{CE} increases from 3.33 to 3.43 V, the I_C and L (red) move forward from point (C) to (A); I_C increases, and L drops because of increased tunneling at higher collector junction bias, but the optical output is still in the coherent emission state with the TL base operates in stimulated recombination. When V_{CE} further increases from 3.43 to 3.51 V, the I_C and L (red) move forward from point (A) to (D); the optical output eventually shifts from coherent to incoherent state when the cavity photon density drops below the coherent threshold ($V_{TU} = 3.46$ V in this case) and the TL base operates in spontaneous recombination, thus the sudden decrease of L. The sudden increase of I_C is due to the higher transistor current gain when the base recombination rate is reduced.

When V_{CE} decreases from 3.51 to 3.43 V, the I_C and L (black) move backward from point (D) to (B); the TL optical output is still in the incoherent state with the base operating in spontaneous recombination. When V_{CE} further decreases from 3.43 to 3.33 V, the I_C and L (black) move backward from point (B) to (C); the TL cavity loss is eventually reduced below the optical gain and the stimulated emission can kickoff, thus the optical output shifts from incoherent to coherent (lasing) at $V_{TU} = 3.4$ V. Thus, we see a TL electro-optical bistability realized and demonstrated as it switches between the coherent state (A) and the incoherent state (B).

The TL electrical and optical output hysteresis observed above are due to the different time delays associated with either photon generation or photon absorption. The time delay for the electrical and optical stepping-up is expected to be shorter due to the fast-tunneling process efficiently reducing the cavity photon density. The tunneling time is estimated to be ∼6 to 8 *fs* measured by field emission microscopy [45] or ∼20 to 50 *fs* by calculation [46]. The time delay for the electrical and optical stepping-down is expected to be longer, owing to the slow photon generation rate via spontaneous *e-h* recombination that is required to build up the cavity photon density to reach coherent state, which is in the picosecond range.

The coherent to incoherent switching behaviors as a function of base current biased dependency in transistor laser family characteristics of collector I_C-V_{CE} and optical L-V_{CE} as shown in previously published ICPAT paper [35]–[42], we have observed the switching occurs at lower collector voltage as base current increases (more coherent photons in the cavity → higher photon-field). This provides the clearly evidence of photon-field enhanced *e-h* tunneling process.

E. Tunneling in Transistor Injected Quantum-Cascade Laser [47]

The transistor-injected quantum cascade laser (TI-QCL) is inspired by the three-terminal transistor laser. The key feature of TI-QCL is to incorporate the active region of QCL between the *p*-type base and the *n*-type collector of an *n-p-n* transistor. The transistor structure allows separate control of current through the quantum cascade active region and voltage drop across the region. This would enable stable spectral output from the electron inter-subband transition and separation of current and voltage modulation.

The inserted quantum cascade region in the base-collector junction also forms a tunable barrier for electrons to transition from the base into collector which controls the radiative base recombination. As the quantum states in the incorporated cascade region align to create decent spatial overlap foe designed inter-subband emission, the impedance to electrons flowing out of base is reduced and so is recombination lifetime. When the quantum states are off-aligned the impedance to electrons escaping the base is enhanced and so is the radiative base recombination. The modulation of the base recombination through the alignment of the quantum states is a unique feature of TI-QCL which promises to have more applications.

VI. Conclusion

The tunneling modulation of the transistor laser is realized by controlling the intra-cavity photon-assisted tunneling (ICPAT) optical absorption at the collector junction with junction bias. Based on analysis of experimental data and knowledge of transistor fundamental operations, we formulated the carrier balance equations in the presence of ICPAT and revealed the inherent electron-photon coupling, which established the transistor laser tunneling operating principles governing both the electrical and the optical outputs.

As a result, the transistor laser's coherent light output can be modulated by either base current injection via stimulated photon generation or base-collector junction voltage bias via optical absorption, making transistor laser a unique two-input laser source. The tunneling modulation scheme, physically limited by the tunneling time (∼femtoseconds), is theoretically much faster than the current modulation which is limited by the carrier recombination lifetime (∼picoseconds); thus, the transistor laser with proper scaling and parasitic reduction is a promising candidate to replace the current generation diode lasers in future high-speed optical links and to push the single-channel direct-modulation data rate to the 100 Gbit/s regime.

Acknowledgement

Since the realization of transistor laser concept in 2003 by Milton Feng and Nick Holonyak, Jr., at the University of Illinois, the authors would like to thank many key contributors. These include Dr. Richard Chan (Qorvo), Dr. Gabriel Water (QEOS), Dr. Han-Wui Then (Intel), Dr. Adam James (Infinera), Dr. Fei Tan (Apple), Professor Chao-Tsin Wu (NTU), Dr. Rohan Bambery (Intel), Dr. Mong-Kai Wu (Intel), Dr. Erik Iverson (Intel), Dr. Michael Liu (Intel), Mr. Curtis Y. Wang, Professor Russell D. Dupuis (GaTech) and Dr. Forest Dixon (Avago) for the long-wavelength TL.

References

[1] J. Bardeen and W. H. Brattain, "The transistor, a semi-conductor triode," *Phys. Rev.*, vol. 74, p. 230, Jul. 1948.
[2] J. S. Kilby, "Invention of the integrated circuit," *IEEE Trans. Electron Devices*, vol. 23, no. 7, pp. 648–654, Jul. 1976.
[3] R. N. Noyce, "Semiconductor device-and-lead structure," U.S. Patent 2 981 877, Apr. 25, 1961.
[4] J. S. Kilby, "Miniaturized electronic circuits," U.S. Patent 3 138 743, Jun. 23, 1964.
[5] W. Shockley, "Circuit element utilizing semiconductive material," U.S. Patent 2 569 347, Sep. 25, 1951.
[6] H. Kroemer, "Theory of a wide-gap emitter for transistors," *Proc. IRE*, vol. 45, no. 11, pp. 1535–1537, Nov. 1957.
[7] W. Snodgrass, W. Hafez, N. Harff, and M. Feng, "Pseudomorphic InP/InGaAs heterojunction bipolar transistors (PHBTs) experimentally demonstrating f_T = 765 GHz at 25°C increasing to f_T = 845 GHz at -55°C," in *IEDM Tech. Dig.*, Dec. 2006, pp. 1–4.
[8] R. N. Hall, G. E. Fenner, J. D. Kingsley, T. J. Soltys, and R. O. Carlson, "Coherent light emission from GaAs junctions," *Phys. Rev. Lett.*, vol. 9, p. 366, Nov. 1962.
[9] N. Holonyak, Jr., and S. F. Bevacqua, "Coherent (visible) light emission from $Ga(As_{1-x}P_x)$ junctions," *Appl. Phys. Lett.*, vol. 1, no. 4, p. 82, 1962.
[10] E. A. Rezek *et al.*, "LPE $In_{1-x}Ga_xP_{1-z}As_z$ (x 0.12, z 0.26) DH laser with multiple thin-layer (<500 Å) active region," *Appl. Phys. Lett.*, vol. 31, no. 4, pp. 288–290, 1977.
[11] R. D. Dupuis, P. D. Dapkus, N. Holonyak, E. A. Rezek, and R. Chin, "Room-temperature laser operation of quantum-well $Ga_{(1-x)}Al_xAs$-GaAs laser diodes grown by metalorganic chemical vapor deposition," *Appl. Phys. Lett.*, vol. 32, no. 1978, p. 295, 1978.
[12] P. Westbergh, E. P. Haglund, E. Haglund, R. Safaisini, J. S. Gustavsson, and A. Larsson, "High-speed 850 nm VCSELs operating error free up to 57 Gbit/s," *Electron. Lett.*, vol. 49, no. 16, pp. 1021–1023, Aug. 2013.
[13] M. Liu, C. Y. Wang, M. Feng, and N. Holonyak, "Advanced development of 850 nm oxide-confined VCSELs with a 57 Gb/s error-free data transmission," GOMAC, Beirut, Lebanon, Tech. Rep. 2016, 2016.
[14] M. Feng, N. Holonyak, Jr., and W. Hafez, "Light-emitting transistor: Light emission from InGaP/GaAs heterojunction bipolar transistors," *Appl. Phys. Lett.*, vol. 84, no. 1, pp. 151–153, 2004.

[15] M. Feng, N. Holonyak, and R. Chan, "Quantum-well-base heterojunction bipolar light-emitting transistor," *Appl. Phys. Lett.*, vol. 84, no. 11, pp. 1952–1954, 2004.
[16] G. Walter, N. Holonyak, M. Feng, and R. Chan, "Laser operation of a heterojunction bipolar light-emitting transistor," *Appl. Phys. Lett.*, vol. 85, no. 20, pp. 4768–4770, 2004.
[17] M. Feng, N. Holonyak, G. Walter, and R. Chan, "Room temperature continuous wave operation of a heterojunction bipolar transistor laser," *Appl. Phys. Lett.*, vol. 87, no. 13, p. 131103, 2005.
[18] G. Walter, C. H. Wu, H. W. Then, M. Feng, and N. Holonyak, "Tilted-charge high speed (7 GHz) light emitting diode," *Appl. Phys. Lett.*, vol. 94, no. 23, p. 231125, 2009.
[19] M. Feng, H. W. Then, N. Holonyak, G. Walter, and A. James, "Resonance-free frequency response of a semiconductor laser," *Appl. Phys. Lett.*, vol. 95, no. 3, p. 033509, 2009.
[20] C. Y. Wang, M. Liu, M. Feng, and N. Holonyak, "Microwave extraction method of radiative recombination and photon lifetimes up to 85 °C on 50 Gb/s oxide-vertical cavity surface emitting laser," *J. Appl. Phys.*, vol. 120, no. 22, p. 223103, 2016.
[21] H. W. Then, M. Feng, and N. Holonyak, "Physics of base charge dynamics in the three port transistor laser," *Appl. Phys. Lett.*, vol. 96, no. 11, p. 113509, 2010.
[22] H. W. Then, M. Feng, and N. Holonyak, "Microwave circuit model of the three-port transistor laser," *J. Appl. Phys.*, vol. 107, no. 9, p. 094509, 2010.
[23] H. W. Then, M. Feng, and N. Holonyak, "Optical bandwidth enhancement by operation and modulation of the first excited state of a transistor laser," *Appl. Phys. Lett.*, vol. 91, no. 18, p. 183505, 2007.
[24] H. W. Then, G. Walter, M. Feng, and N. Holonyak, "Collector characteristics and the differential optical gain of a quantum-well transistor laser," *Appl. Phys. Lett.*, vol. 91, no. 24, p. 243508, 2007.
[25] H. W. Then, F. Tan, M. Feng, and N. Holonyak, "Transistor laser optical and electrical linearity enhancement with collector current feedback," *Appl. Phys. Lett.*, vol. 100, no. 22, p. 221104, 2012.
[26] M. Feng, N. Holonyak, H. W. Then, C. H. Wu, and G. Walter, "Tunnel junction transistor laser," *Appl. Phys. Lett.*, vol. 94, no. 4, p. 041118, 2009.
[27] H. W. Then, C. H. Wu, G. Walter, M. Feng, and N. Holonyak, "Electrical-optical signal mixing and multiplication (2→22 GHz) with a tunnel junction transistor laser," *Appl. Phys. Lett.*, vol. 94, no. 10, p. 101114, 2009.
[28] M. Feng and N. Holonyak, "The Metamorphosis of the transistor into a laser," *Opt. Photon. News*, vol. 22, no. 3, pp. 44–49, Mar. 2011.
[29] H. W. Then, M. Feng, and N. Holonyak, "The transistor laser: Theory and experiment," *Proc. IEEE*, vol. 10, no. 101, pp. 2271–2298, Oct. 2013.
[30] L. V. Keldysh, "The effect of a strong electric field on the optical properties of insulating crystals," *Sov Phys. JETP*, vol. 7, no. 5, pp. 1138–1141, 1958.
[31] J. Callaway, "Optical absorption in an electric field," *Phys. Rev.*, vol. 130, no. 2, pp. 549–553, 1963.
[32] K. Tharmalingam, "Optical absorption in the presence of a uniform field," *Phys. Rev.*, vol. 130, pp. 2204–2206, Jun. 1963.
[33] C. M. Wolfe and N. Holonyak, *Physical Properties of Semiconductors*. Englewood Cliffs, NJ, USA: Prentice-Hall, 1989.
[34] G. E. Stillman and C. M. Wolfe, "Avalanche photodiodes," in *Infrared Detector, Semiconductors and Semimetals*, vol. 12. San Francisco, CA, USA: Academic, 1977, pp. 291–391.
[35] A. James, J. Holonyak, M. Feng, and G. Walter, "Franz–Keldysh photon-assisted voltage-operated switching of a transistor laser," *IEEE Photon. Technol. Lett.*, vol. 19, no. 9, pp. 680–682, May 2007.
[36] M. Feng, N. Holonyak, H. W. Then, C. H. Wu, and G. Walter, "Tunnel junction transistor laser," *Appl. Phys. Lett.*, vol. 94, no. 4, pp. 1–4, 2009.
[37] H. W. Then, C. H. Wu, G. Walter, M. Feng, and N. Holonyak, "Electrical-optical signal mixing and multiplication (2→22 GHz) with a tunnel junction transistor laser," *Appl. Phys. Lett.*, vol. 94, no. 10, pp. 1–4, 2009.
[38] H.-L. Wang, Y.-H. Huang, G.-S. Cheng, S.-W. Chang, and C.-H. Wu, "Analysis of tunable internal loss caused by Franz–Keldysh absorption in transistor lasers," *IEEE J. Sel. Topics Quantum Electron.*, vol. 21, no. 6, Dec. 2015, Art. no. 1503007.
[39] M. Feng, J. Qiu, C. Y. Wang, and N. Holonyak, "Intra-cavity photon-assisted tunneling collector-base voltage-mediated electron-hole spontaneous-stimulated recombination transistor laser," *J. Appl. Phys.*, vol. 119, no. 8, p. 84502, 2016.
[40] M. Feng, J. Qiu, C. Y. Wang, and N. Holonyak, "Tunneling modulation of a quantum-well transistor laser," *J. Appl. Phys.*, vol. 120, no. 20, p. 204501, 2016.
[41] M. Feng, R. Bambery, and N. Holonyak, "Band-filling and photon-assisted tunneling in a quantum-well transistor laser," *Appl. Phys. Lett.*, vol. 98, no. 12, p. 123505, 2011.
[42] M. Feng, C.-H. Wu, C.-H. Wu, and N. Holonyak, "Resonance-free optical response of a vertical cavity transistor laser," *Appl. Phys. Lett.*, vol. 111, no. 12, p. 121106, 2017.
[43] Y. Xiang *et al.*, "Performance optimization of GaAs-based vertical-cavity surface-emitting transistor-lasers," *IEEE Photon. Technol. Lett.*, vol. 27, no. 7, pp. 721–724, Apr. 1, 2015.
[44] M. Feng, N. Holonyak, and C. Y. Wang, "Room temperature operation of electro-optical bistability in the edge-emitting tunneling-collector transistor laser," *J. Appl. Phys.*, vol. 122, no. 10, p. 103102, 2017.
[45] S. K. Sekatskii and V. S. Letokhov, "Electron tunneling time measurement by field-emission microscopy," *Phys. Rev. B, Condens. Matter*, vol. 64, no. 23, p. 233311, 2001.
[46] Z. S. Wang, L. C. Kwek, C. H. Lai, and C. H. Oh, "Quantum tunneling time," *Phys. Rev. A-Atom. Mol. Opt. Phys.*, vol. 69, no. 5, p. 52108, 2004.
[47] K. Chan and J. M. Dallesasee, "Design and modeling of mid-infrared transistor-injected quantum cascade lasers," in *Proc. Int. Conf. Compound Semiconductor Manuf. Technol.*, Denver, CO, USA, May 2014, pp. 75–78.

Milton Feng (F'92–LF'17) received the B.S. degree in electrical engineering from Columbia University, New York, in 1973, and the M.S. and Ph.D. degrees in electrical engineering from the University of Illinois at Urbana–Champaign, in 1976 and 1979, respectively. From 1984 to 1986, he was with Ford Microelectronics, Inc., Colorado Springs, CO, USA, where he managed the advanced digital integrated circuit development program in 1-K SRAM and 500 gate arrays. From 1979 to 1983, he was the Head of the Torrance Research Center, GaAs Material and Device Group, Hughes Aircraft Company, where he was in charge of ion implantation, $AsCl_3$ VPE, MOCVD, and MBE technology. In 1983, he developed a direct ion-implanted low-noise and power MESFET and MMICs for *X*-band phase array radar application. He demonstrated the first 60-GHz GaAs amplifiers in 1983.

Since 1991, he has been a Professor of electrical and computer engineering and a Research Professor with the Microelectronics Laboratory, University of Illinois, where he is currently the Holonyak Endowed Chair Professor of electrical and computer engineering. He invented the pseudomorphic HBT (PHBT), "pushed" the transistor speed boundary toward THz, and demonstrated InP PHBTs with the world's fastest speed performance (> 800 GHz). He, along with Prof. N. Holonyak, Jr., demonstrated the first laser operation of a quantum-well-based light emitting transistor, a transistor laser. A transistor laser opens up a rich domain of integrated circuitry and high-speed signal processing that involves both electrical and optical signals.

He has published over 250 papers, 220 conference talks, and he holds 39 U.S. patents in semiconductor microelectronics and photonics. He is an OSA Fellow. He serves on many executive and strategy committees both in industry and at conferences. He received the Ford Aerospace Corporate Technology Outstanding Principal Investigator Award for his contribution of advancing ion implantation GaAs and InGaAs MESFETs into manufacturable millimeter-wave ICs in 1989, the IEEE Field Award—David Sarnoff Award in 1997, and the Pan Wen Yuan Outstanding Research Award in microelectronics in 2000. In 2005, he was chosen as the first Holonyak Chair Professor of electrical and computer engineering. In 2006, his transistor laser research paper was selected as one of the top five papers in the 43-year history of *Applied Physics Letters* and was also selected as one of the top 100 most important discoveries in 2005 by *Discover* magazine. In 2013, he received the Optical Society R. W. Wood Prize for the co-invention and realization of the transistor laser. In 2017, he was a recipient of the Distinguished ECE Alumni Award at the University of Illinois.

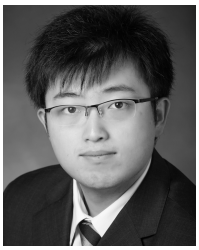

Junyi Qiu (SM'16) received the B.S. and M.S. degrees in electrical engineering from the University of Illinois at Urbana–Champaign in 2013 and 2016, respectively. He is currently pursuing the Ph.D. degree, under the supervision of Prof. M. Feng, in high-speed electronics, including THz InP HBT, high-speed VCSEL optical links, and transistor laser-based next-generation optical systems. He received the John Bardeen Graduate Fellowship in 2015 and the Nick and Katherine Holonyak, Jr., Graduate Student Fellowship from the University of Illinois in 2017.

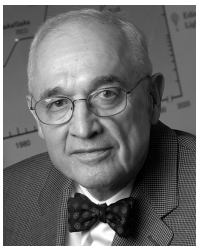

Nick Holonyak, Jr. (LF'94) was born in Zeigler, IL, USA, in 1928. He received the B.S., M.S., and Ph.D. degrees from the University of Illinois in 1950, 1951, and 1954, respectively, all in EE. He was John Bardeen's first student and held the TI Fellowship. He was with Bell Telephone Laboratories from 1954 to 1955. After military service, he was with GE, Syracuse, NY, USA, from 1957 to 1963, before returning to the University of Illinois in 1963, where he is currently the John Bardeen Chair Professor of electrical and computer engineering and physics, and an ECE Professor with the Center of Advanced Study.

From 1954 to 1960, he was an early Contributor to diffused-impurity oxide-masked silicon device technology (transistors, p-n-p-n switches, and thyristors), the technology basic to the integrated circuit. In 1958, he was the Inventor of the shorted emitter used in thyristors and symmetrical switches, including the basic element in the wall light dimmer. He was the first to make silicon tunnel diodes and observe phonon-assisted tunneling in 1959, the first observation of ineleastic tunneling and the beginning of tunneling spectroscopy. He invented the closed-tube vapor phase epitaxy of III–V semiconductors in 1960 and the forerunner of present-day open-tube III–V VPE crystal growth. Besides early work on III–V heterojunctions from 1960 to 1962, he was the first to grow $GaAs_{1-x}P_x$ (an alloy) in 1960 and to construct visible-spectrum lasers and light emitting diodes in 1962, thus proving that III–V alloys are smooth and viable, in general, for use in optoelectronic devices. He was the inventor of the first practical LED, the red $GaAs_{1-x}P_x$ LED, which (based on its diode laser extension) led to the concept of an ultimate lamp and also marked the beginning in the use of III–V alloys in semiconductor devices, including in heterojunctions and quantum well heterostructures (QWHs). Besides demonstrating the visible-spectrum laser operation of the alloys GaAsP (1962), InGaP (1970), AlGaAsP (1970), and InGaPAs (1972), he and his student Rezek made (via LPE, 1977) the first QW diode lasers. Later, with Dupuis (and MOCVD AlGaAs-GaAs), he demonstrated an initial continuous 300-K operation of a QW laser in 1978 and introduced the name quantum well laser. In 1980, he and his students introduced impurity-induced disordering and intermixing ($\sim$ 600 °C) of QWH and superlattice layers, and with it the selective shift from QW lower gap to bulk-crystal higher gap (used to define waveguide and laser geometries). In 1990, he and his students introduced the Al-based III–V native oxide into optoelectronics, including its use as a buried oxide aperture to define the current and cavity in lasers (now used in VCSELs). He (with Dupuis) introduced coupled quantum-dot/quantum-well lasers, and with M. Feng introduced light-emitting heterojunction bipolar transistors modified with quantum-well base regions and re-invented the transistor as a transistor laser in 2004. His work has led to over 574 papers and 55 patents.

Dr. Holonyak was a member of the National Academy of Engineering in 1973 and the National Academy of Sciences in 1984, a fellow of the American Academy of Arts and Sciences in 1984, a Foreign Member of the Russian Academy of Sciences in 1999, a fellow of the American Physical Society, a Life Fellow of the Institute of Electrical and Electronics Engineers, a fellow of the Optical Society of America, a fellow of the American Association for the Advancement of Science, a member of the Electrochemical Society, and a member of the Mathematical Association of America. He received a number of awards, including the Cordiner Award from GE in 1962, the Morris N. Liebmann Award from the IEEE in 1973, the John Scott Medal at Philadelphia in 1975, the Gallium Arsenide Symposium Award with the Welker Medal in 1976, the Jack A. Morton Award from the IEEE in 1981, the Solid State Science and Technology Award from the Electrochemical Society in 1983, the Monie A. Ferst Award from the Sigma Xi in 1988, the Edison Medal from the IEEE in 1989, the National Medal of Science at USA in 1990, the Charles H. Townes Award from OSA in 1992, an Honorary Member of the Ioffe Physical-Technical Institute, Saint Petersburg, in 1992, the Honorary Doctor of Science from Northwestern University in 1992, the NAS Award for the Industrial Application of Science in 1993, the ASEE Centennial Medal in 1993, the American Electronics Association 50th Anniversary Award in 1993, the Vladimir Karapetoff Eminent Members' Award of the Eta Kappa Nu in 1994, the Honorary Doctor of Engineering from the University of Notre Dame in 1994, the TMS John Bardeen Award from The Minerals, Metals, and Materials Society in 1995, the Japan Prize in 1995, an Eminent Member of the Eta Kappa Nu in 1998, the Distinguished Alumnus of the Tau Beta Pi in 1999, the IEEE Third Millennium Award in 2000, the Frederic Ives Medal of the Optical Society of America in 2001, the Global Energy International Prize at Russia in 2003, the IEEE Medal of Honor in 2003, the National Medal of Technology Medal in 2002, the National Medal of Technology Award in 2003, the Washington Award from the Western Society of Engineers in 2004, the Lemelson—MIT Prize in 2004, the MRS Von Hippel Award in 2004, the Izaak Walton League of America Illinois Division Energy Conservation Award in 2004, a Laureate of The Lincoln Academy of Illinois in 2005, a member of the Consumer Electronics Association Hall of Fame in 2006, the National Inventors Hall of Fame in 2008, The Engineering at Illinois Hall of Fame in 2010, Engineering and Science Hall of Fame in 2011. In 2015, he was a recipient of the NAE Charles Stark Draper Prize, and he was elected to a prestigious OSA Honorary Member.